IJRCS

International Journal of Robotics and Control Systems
Vol. 5, No. 6, 2025, pp. 2685-2708
ISSN 2775-2658
http://pubs2.ascee.org/index.php/ijrcs

ASCEE

Integration of Hybrid Active Disturbance Rejection with Sliding Mode Control for Robust Mechanical Ventilation

Mohammed Albaker Najm Abed [a,1,*], Zubaidah Saleem Hasan [b,2], Ahmed Zurfi [c,3]

[a] Department of Computer Technology Engineering, Al Taff University College, Karbala, 56001, Iraq
[b] College of Engineering and Information Technology, Al-Zahraa University for Women, Karbala, Iraq
[c] Department of Electrical Engineering Techniques, Al-Hussain University College, Karbala, Iraq
[1] eng.mohammed.iq99@gmail.com; [2] zubaida.salim@alzahraa.edu.iq; [3] ahmed.jabbar@uokerbala.edu.iq
* Corresponding Author

ARTICLE INFO

Article history
Received July 27, 2025
Revised August 28, 2025
Accepted November 26, 2025

Keywords
Active Disturbance Rejection Control (ADRC);
Sliding Mode Control (SMC);
Non-Linear PD Controller;
Mechanical Ventilation;
Respiratory System

ABSTRACT

This study addresses the challenge of precise control within the human respiratory system, a complex, nonlinear, and time-varying physiological process. The research contribution is to develop and evaluate a robust hybrid controller that integrates Active Disturbance Rejection Control (ADRC) with Sliding Mode Control (SMC) to overcome the limitations of traditional control methods. The respiratory system's behavior is modeled as a state-space system, where internal and external disturbances, such as changes in lung mechanics, patient effort, and environmental factors, can significantly impact performance. We conducted a series of simulations to validate the effectiveness of the proposed controller. The hybrid ADRC-SMC controller was rigorously compared with ADRC using a nonlinear PD controller (ADRC-NPD) across various simulated scenarios. The results demonstrate that the ADRC-SMC responds better than the ADRC-NPD. The ADRC-SMC achieved a settling time of 0.3 seconds, a rise time of 0.1 seconds, and a tracking efficiency exceeding 98%, outperforming the ADRC-NPD. While traditional SMC often suffers from chattering, the ADRC component effectively mitigates this issue by estimating and compensating for disturbances, resulting in smoother control signals and reduced torque ripple. The advanced ADRC-SMC controller effectively regulates the respiratory system, offering superior performance and robustness against disturbances. The key limitation is the inherent computational complexity of the ADRC algorithm, which may pose challenges for real-time implementation on low-power hardware. While the hybrid approach reduced chattering, a small degree of control effort oscillation remains, warranting further investigation into advanced techniques for reducing chattering. Future work will optimize the algorithm's efficiency and expand its clinical applications for greater generalizability.

1. Introduction

The respiratory system, a vital physiological network, is responsible for the critical process of gas exchange, enabling the intake of oxygen and the expulsion of carbon dioxide [1], [2]. Its

classification can broadly encompass natural biological respiration and artificially supported systems, such as mechanical ventilators, each profoundly impacting patient well-being, from maintaining physiological homeostasis to aiding recovery in critical conditions [3], [4]**.** The system functionality is inherently influenced by numerous factors, including varying lung compliance, dynamic airway resistance, patient effort, and external disturbances, all of which introduce significant complexities such as nonlinearity and uncertainty [5], [6].

To effectively manage and support the dynamic biological system, particularly in cases that require mechanical ventilation, robust control methods are essential [7], [8]. Historically, Proportional-Integral-Derivative (PID) controllers have provided foundational control [9]-[13]. At the same time, more advanced techniques, such as Sliding Mode Control (SMC) and Nonlinear Proportional-Derivative (NPD) methods, have offered enhanced robustness against disturbances. Recently, Active Disturbance Rejection Control (ADRC) has emerged as a powerful model-free approach capable of estimating and compensating for unknown dynamics [14]-[19].

The primary scientific gap in the existing literature is the lack of a comprehensive validated study on a hybrid control strategy that effectively integrates the robustness of SMC with the disturbance rejection capabilities of ADRC for managing the complex, time-varying dynamics of the respiratory system [20]-[24]. While individual control strategies have been explored the literature lacks rigorous analysis of a combined approach that simultaneously minimizes chattering, maintains high tracking efficiency, and manages a variety of physiological disturbances in a unified framework.

This gap is particularly evident in the absence of a detailed comparison of such a hybrid model against traditional methods especially concerning key performance metrics like settling time, rise time, and control effort [25], [26]. The specific hybrid configurations, ADRC-NPD and ADRC-SMC, were chosen for their complementary strengths in addressing the unique challenges of respiratory system control. ADRC is a model-free approach that excels at estimating and compensating for both internal and external disturbances in real-time. That is crucial for a system like the respiratory system where disturbances arise from patient effort, changes in lung compliance and resistance, and sensor noise. Its NPD feedback law provides an intuitive and effective way to manage tracking errors [27]-[31].

The integration with SMC was selected because SMC offers exceptional robustness to parameter uncertainties and unmodeled dynamics. In a biomedical system with inherent patient variability, the robustness is a significant advantage. The hybrid ADRC-SMC configuration leverages ADRC ability to reduce the chattering often associated with SMC by providing a smoothed, disturbance-compensated control signal. These hybrid controllers were chosen for their unique ability to combine effective disturbance rejection with high robustness that minimizing the need for precise system models while simultaneously mitigating common pitfalls of each individual method. A primary concern is real-time implementability due to the high computational complexity of the ADRC algorithm particularly its Extended State Observer (ESO).

The ESO requires substantial processing power to accurately estimate disturbances which may exceed the capabilities of low-cost, embedded microcontrollers typically used in portable mechanical ventilators. Additionally the performance of the controller is highly susceptible to sensor noise. While ESO robust it can be sensitive to high-frequency noise in the airway pressure and patient flow signals potentially leading to inaccurate disturbance estimation and degraded control performance. Finally the simulations were based on an idealized physiological model; the controller's effectiveness in a real-world clinical environment, which involves a broader spectrum of patient variability and unmodeled physiological events that remains to be more accurate in implementation.

The rest of the paper is organized as follows: Section 2 presents the methodology and mathematical model, including the respiratory system, ADRC, ADRC- NPID, and ADRC-SMC. Section 3 presents the numerical results of the simulation for each scenario, along with a corresponding description. Section 4 outlines the conclusion, future works, and references.

2. Methodology

2.1. Respiratory System

The human respiratory system, which is fundamentally responsible for gas exchange [32], is a complex biological network comprising the lungs, airways, and respiratory muscles, all working in concert to facilitate the intake of oxygen and the expulsion of carbon dioxide [33]. Its intricate dynamics, including varying lung compliance, airway resistance, and the active involvement of muscles for breathing, lend themselves well to representation as a state-space model [34]. In such a model, the system behavior is described by a set of first-order differential equations that define its internal states. For the respiratory system, key state variables might include lung volume, airway pressure (P_{aw}), and patient flow (Q_{pat}). These states evolve based on inputs like ventilator pressure or flow commands and are influenced by system parameters that can change due to physiological conditions or external disturbances [35]. The state-space representation enables a systematic analysis of the system response to various inputs and disturbances, making it a powerful tool for understanding respiratory mechanics and designing advanced control strategies, such as those used in mechanical ventilation, where controllers aim to manipulate inputs to achieve desired state trajectories for patient well-being. Table 1. shows the ventilator parameters used in the research [36], [37]. Fig. 1 shows the closed loop control system for the respiratory system.

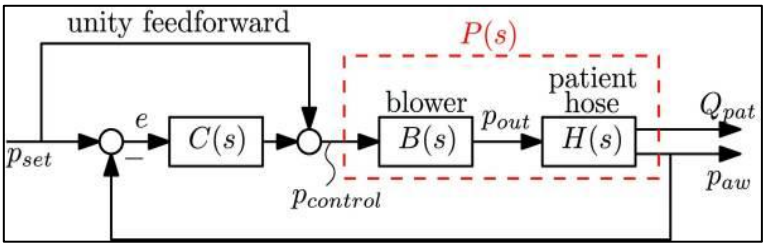

Fig. 1. Depicts a closed-loop control system for mechanical ventilation

The lungs draw in air at an airflow rate of (Q_o) and concurrently release a flow rate of (Q_{leak}) through a leaky hose, leaving (Q_{pat}) as the remaining exhaled airflow [36].

$$Q_{pat} = Q_o - Q_{leak} \tag{1}$$

An electric circuit is a similar concept for the respiratory system. where resistances represent obstacles to airflow, pressures correspond to voltage, and airflow resembles electric current. Using Ohm's law [38], the patient's airflow can be mathematically represented with a pressure sensor measuring airway pressure (P_{aw}). The control system's primary goal is to ensure that the measured pressure accurately tracks the intended set point (P_r), leading to the formulation of an error equation to achieve precise pressure regulation [39]:

$$e = P_r - P_{aw} \tag{2}$$

The conventional resistances connected to the hose can be used to indicate the blower (Q_o), patient (Q_{pat}), and leak (Q_{leak}) flow rates, leak channel, and the patient lungs as shown:

$$\left.\begin{aligned} Q_o &= \frac{P_o - P_{aw}}{R_h} \\ Q_{leak} &= \frac{P_{aw}}{R_{leak}} \\ Q_{pat} &= \frac{P_{aw} - P_{lung}}{R_{lung}} \end{aligned}\right\} \tag{3}$$

The blower output pressure is denoted by P_o, the airway pressure by P_{aw}, the hose resistance by R_h, the resilience of the leak by R_{leak}, and the lung resistance by R_{lung}. Lung dynamics and lung pressure P_{lung} satisfy the following differential equation.

$$P_{lung} = \frac{1}{C_{lung}} . Q_{pat} \tag{4}$$

where lung compliance (elastance) is denoted by C_{lung}. Equation (3) Q_{pat} is equal to current and P_{lung} is equal to voltage. The following expression can be obtained by substituting equation (3) into equation (4):

$$P_{lung} = \frac{P_a - P_{lung}}{C_{lung}. R_{lung}} \tag{5}$$

The airway pressure (in Pascals) can be obtained rewrite the airway pressure equation by substituting (3) into (1). This will yield in (6).

$$P_{aw} = \frac{\frac{1}{R_h}. P_o + \frac{1}{R_{lung}}. P_{lung}}{\frac{1}{R_{lung}} + \frac{1}{R_h} + \frac{1}{R_{leak}}} \tag{6}$$

The following updated equation is obtained by substituting the airway pressure expression from (6) into the lung dynamics equation in (5):

$$P_{lung} = \frac{-P_{lung}\left(\frac{1}{R_h} + \frac{1}{R_{leak}}\right) + \frac{1}{R_h}. P_o}{C_{lung}. R_{lung}\left(\frac{1}{R_{lung}} + \frac{1}{R_h} + \frac{1}{R_{leak}}\right)} \tag{7}$$

Equations (3), (6), and (7) can be used to model the patient and hose system as a linear state-space system with P_o. serving as both the input and the output. $\begin{bmatrix} P_{aw} \\ Q_{pat} \end{bmatrix}$, and P_{lung} is the state.

$$P_{lung} = A_h P_{lung} + B_h P_o \tag{8}$$

$$\begin{bmatrix} P_{aw} \\ Qpat \end{bmatrix} = C_h P_{lung} + D_h P_o \tag{9}$$

where:

$$\left.\begin{aligned} A_h &= -\frac{\frac{1}{R_h} + \frac{1}{R_{leak}}}{C_{lung}. R_{lung}\left(\frac{1}{R_{lung}} + \frac{1}{R_h} + \frac{1}{R_{leak}}\right)} \\ B_h &= \frac{\frac{1}{R_h}}{C_{lung}. R_{lung}\left(\frac{1}{R_{lung}} + \frac{1}{R_h} + \frac{1}{R_{leak}}\right)} \\ C_h &= \begin{bmatrix} \frac{\frac{1}{R_{lung}}}{\frac{1}{R_{lung}} + \frac{1}{R_h} + \frac{1}{R_{leak}}} \\ -\frac{\frac{1}{R_h} + \frac{1}{R_{leak}}}{R_{lung}\left(\frac{1}{R_{lung}} + \frac{1}{R_h} + \frac{1}{R_{leak}}\right)} \end{bmatrix} \\ D_h &= \begin{bmatrix} \frac{\frac{1}{R_h}}{\frac{1}{R_{lung}} + \frac{1}{R_h} + \frac{1}{R_{leak}}} \\ \frac{\frac{1}{R_h}}{R_{lung}\left(\frac{1}{R_{lung}} + \frac{1}{R_h} + \frac{1}{R_{leak}}\right)} \end{bmatrix} \end{aligned}\right\} \tag{10}$$

Alternatively, it can be represented in transfer function notation as follows:

$$H(s) = C_h \frac{1}{(\mathrm{SI}-\mathrm{A_h})} \mathrm{B_h} + \mathrm{D_h} \tag{11}$$

where:

$$A_h = -\frac{\frac{1}{0.0045}+\frac{1}{0.06}}{0.005*20(\frac{1}{0.005}+\frac{1}{0.0045}+\frac{1}{0.06})} = -5.443 \tag{12}$$

$$B_h = \frac{\frac{1}{0.0045}}{0.005*20(\frac{1}{0.005}+\frac{1}{0.0045}+\frac{1}{0.06})} = 5.0632 \tag{13}$$

$$\mathrm{C_h} = \begin{bmatrix} \frac{\frac{1}{0.005}}{\frac{1}{0.005}+\frac{1}{0.0045}+\frac{1}{0.06}} \\ -\frac{\frac{1}{0.0045}+\frac{1}{0.06}}{0.005(\frac{1}{0.005}+\frac{1}{0.0045}+\frac{1}{0.06})} \end{bmatrix} = \begin{bmatrix} 0.4557 \\ -108.8615 \end{bmatrix} \tag{14}$$

$$\mathrm{D_h} = \begin{bmatrix} \frac{\frac{1}{0.0045}}{\frac{1}{0.005}+\frac{1}{0.0045}+\frac{1}{0.06}} \\ \frac{\frac{1}{0.0045}}{0.005(\frac{1}{0.005}+\frac{1}{0.0045}+\frac{1}{0.06})} \end{bmatrix} = \begin{bmatrix} 0.50633 \\ 101.266 \end{bmatrix} \tag{15}$$

$$\begin{cases} A_b = \begin{bmatrix} -376.8 & -35494.56 \\ 1 & 0 \end{bmatrix} \\ B_b = \begin{bmatrix} 1 \\ 0 \end{bmatrix} \\ C_b = \begin{bmatrix} 0 & 35494.56 \end{bmatrix} \end{cases} \tag{16}$$

$$\begin{cases} \mathrm{A_p} = \begin{bmatrix} -376.8 & -35494.56 & 0 \\ 1 & 0 & 0 \\ 0 & 179716.0562 & -5.443 \end{bmatrix} \\ \mathrm{B_p} = \begin{bmatrix} 1 \\ 0 \\ 0 \end{bmatrix} \\ \mathrm{C_p} = \begin{bmatrix} 0 & 17971.96056 & 0.4557 \\ 0 & 3594392.113 & -108.8615 \end{bmatrix} \end{cases} \tag{17}$$

Table 1 provides a concise summary of the key physiological and mechanical parameters used to model a ventilator system, sourced from a reference indicated in [40]. It details six specific variables essential for simulating the dynamics of mechanical ventilation. These include lung resistance (R_{lung}) and lung compliance (C_{lung}) which are fundamental to describing the mechanical properties of the patient's respiratory system. The table also lists resistances related to the equipment, such as leak resistance (R_{leak}) and hose resistance (R_h), which account for air loss and the properties of the tubing. Finally, it includes the system's natural frequency (ω_n) and damping ratio (ζ) which characterize the overall dynamic response of the modeled system. The table's structure clearly presents the Name, numerical value, Unit, and a brief Parameter description for each entry that offering a complete set of values for simulation purposes [41], [42]. where:

$$A_h = -\frac{\frac{1}{0.0045}+\frac{1}{0.06}}{0.005*20(\frac{1}{0.005}+\frac{1}{0.0045}+\frac{1}{0.06})} = -5.443 \tag{18}$$

$$B_h = \frac{\frac{1}{0.0045}}{0.005*20(\frac{1}{0.005}+\frac{1}{0.0045}+\frac{1}{0.06})} = 5.0632 \tag{19}$$

$$C_h = \begin{bmatrix} \frac{\frac{1}{0.005}}{\frac{1}{0.005}+\frac{1}{0.0045}+\frac{1}{0.06}} \\ -\frac{\frac{1}{0.0045}+\frac{1}{0.06}}{0.005(\frac{1}{0.005}+\frac{1}{0.0045}+\frac{1}{0.06})} \end{bmatrix} = \begin{bmatrix} 0.4557 \\ -108.8615 \end{bmatrix} \tag{20}$$

$$D_h = \begin{bmatrix} \frac{\frac{1}{0.0045}}{\frac{1}{0.005}+\frac{1}{0.0045}+\frac{1}{0.06}} \\ \frac{\frac{1}{0.0045}}{0.005(\frac{1}{0.005}+\frac{1}{0.0045}+\frac{1}{0.06})} \end{bmatrix} = \begin{bmatrix} 0.50633 \\ 101.266 \end{bmatrix} \tag{21}$$

$$\begin{cases} A_b = \begin{bmatrix} -376.8 & -35494.56 \\ 1 & 0 \end{bmatrix} \\ B_b = \begin{bmatrix} 1 \\ 0 \end{bmatrix} \\ C_b = \begin{bmatrix} 0 & 35494.56 \end{bmatrix} \end{cases} \tag{22}$$

$$\begin{cases} A_p = \begin{bmatrix} -376.8 & -35494.56 & 0 \\ 1 & 0 & 0 \\ 0 & 179716.0562 & -5.443 \end{bmatrix} \\ B_p = \begin{bmatrix} 1 \\ 0 \\ 0 \end{bmatrix} \\ C_p = \begin{bmatrix} 0 & 17971.96056 & 0.4557 \\ 0 & 3594392.113 & -108.8615 \end{bmatrix} \end{cases} \tag{23}$$

Table 1. Parameters of the ventilator system

Name	Value	Unit	Parameter
R_{lung}	0.005	$\frac{mbar}{mL/s}$	Lung resistance
C_{lung}	20	$\frac{mL}{mbar}$	Lung's compliance (Capacitance)
R_{leak}	0.06	$\frac{mbar}{mL/s}$	Leak resistance
R_h	0.0045	$\frac{mbar}{mL/s}$	Hose resistance
ω_n	376.8	rad/s	Natural frequency
$\zeta = 1$	1		Damping ratio

2.2. Active Disturbance Rejection Control

Active Disturbance Rejection Control (ADRC) is a model-free control method designed for complex systems with unknown dynamics and disturbances [43]. Its core principle is to estimate and cancel a "total disturbance" that combines all unknown factors [44]. ADRC has three main parts: a Tracking Differentiator (TD) that creates a smooth reference signal; an Extended State Observer (ESO), which is the key component that estimates both the system's states and the total disturbance

in real-time; and a Nonlinear State Error Feedback (NLSEF) control law that uses these estimates to generate the control output, effectively canceling the disturbance [45]-[50]. This structure gives ADRC its notable robustness and adaptability to varying system conditions. The ADRC structure of the respiratory system is shown in Fig. 2.

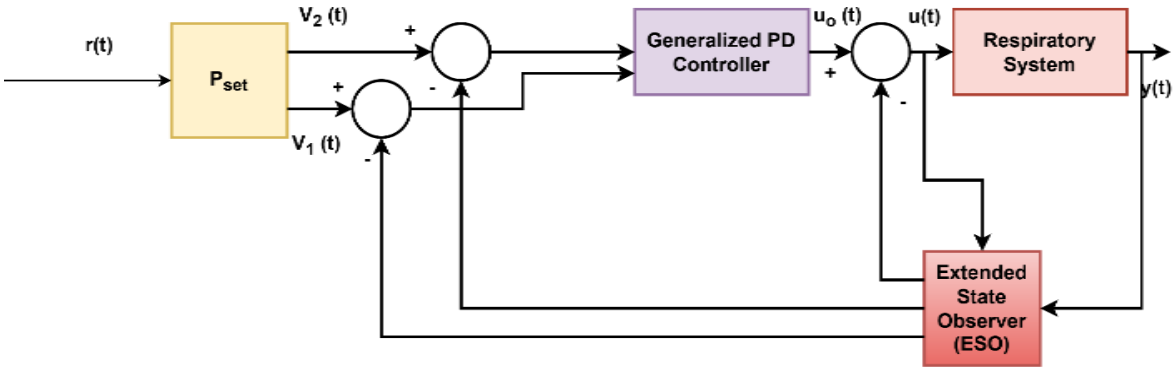

Fig. 2. Block diagram of an active disturbance rejection control system for respiratory control

2.3. ADRC-NPD

Represents an ADRC system where the Nonlinear State Error Feedback (NLSEF) control law is based on an NPD structure [51]. In the provided configuration, the estimated states and the compensated total disturbance from the ESO are fed into a control law that resembles a modified PD controller but with nonlinear gains or functions. While the ADRC fundamental disturbance rejection capabilities remain present due to the ESO, the NPD control law, by its nature, may offer a good initial response; however, it may not possess the same level of aggressive and robust corrective action required for highly dynamic or severely uncertain systems. When applied to a respiratory system [52], ADRC-NPD would aim to control P_{aw} or Q_{pat} [53]. However, due to the less stringent control enforcement of its NPD element compared to other advanced control laws, it might exhibit noticeable overshoot during setpoint changes, slightly longer settling times, and larger instantaneous tracking errors, especially when confronted with sudden patient efforts or abrupt changes in lung mechanics Its effect on the system, while an improvement over basic PID, may still exhibit transient imperfections, such as oscillations, before finally stabilizing the respiratory parameters. Fig. 3 shows the structure of ADRC-NPD.

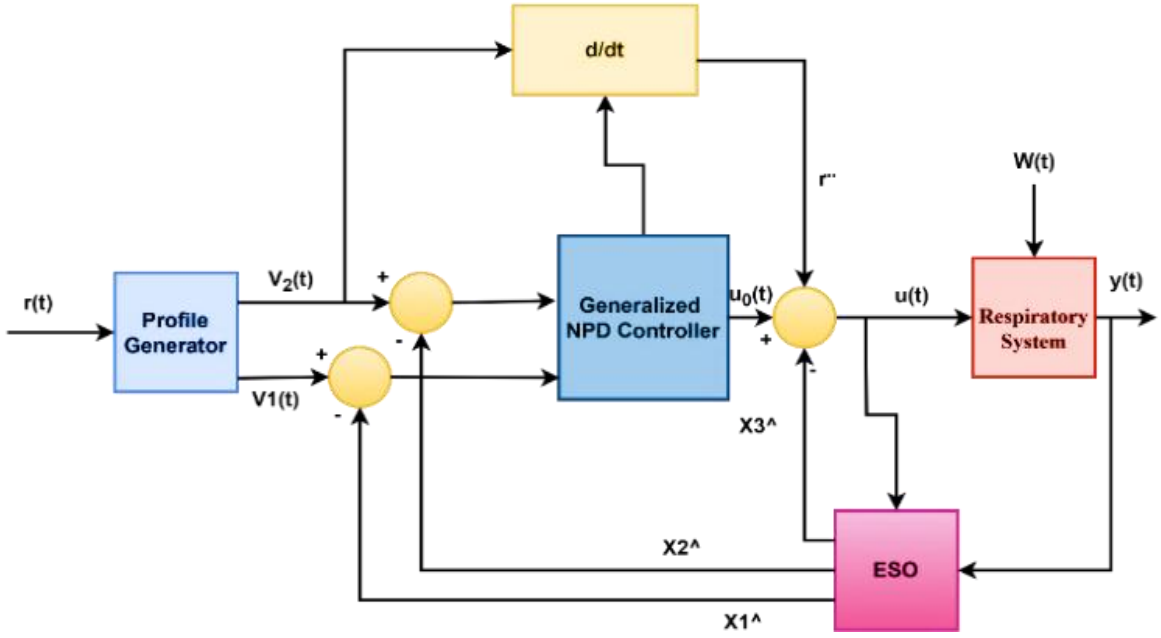

Fig. 3. ADRC-NPD controller block diagram

Equation (24) defines V_2 as the derivative of V_1. In the context of a tracking differentiator, if V_1 is tracking a signal, then V_2 would be its estimated first derivative.

$$\dot{V}_1 = V_2 \tag{24}$$

That is a nonlinear dynamics equation for the second state V_2. Here, r represents the reference signal that V_1 is trying to track. The term $-\varphi$sign(V_1-r) introduces an intense, discontinuous control action based on the sign of the error between V_1 and the reference. The term $\frac{V_2|V_2|}{2\varphi}$ provides damping proportional to the square of V_2, helping to smooth the derivative estimation and prevent chattering.

$$\dot{V}_1 = -\varphi sign\,(V_1 - r + \frac{V_2|V_2|}{2\varphi}) \tag{25}$$

$$\dot{V}_1 = V_2 \tag{26}$$

$$\dot{V}_1 = -\varphi^2 \tanh\left(\frac{\rho V_1 - (1-\varepsilon)r}{\gamma}\right) - \varphi V_2 \tag{27}$$

The parameters $\rho, \varepsilon, \gamma$ are suitable design specifications, where $0 < \varepsilon < 1$, $\rho > 0$ $\gamma > 0$, and $\varphi > 0$. Equation (27) can be modified by making some an assumption as:

$$\dot{V}_1 = V_2 \tag{28}$$

$$\dot{V}_1 = -\varphi^2 \left(\frac{\rho V_1 - (1-\varepsilon)r}{\gamma}\right) - \varphi V_2 \tag{29}$$

It enhances trajectory tracking performance and is better than the conventional nonlinear tracking differentiator. For (ADRC-NPD), in (29) can be written after adding nonlinear function as:

$$\begin{cases} e_1 = (r - \widehat{x_1}) \\ e_2 = (\dot{r} - \widehat{x_2}) \\ u_0 = K_p fal(e_1, \sigma_1, \delta) + K_d\, fal\,(e_2, \sigma_2, \delta) \\ u = \dfrac{u_0 - \hat{x}_3}{b_0} \end{cases} \tag{30}$$

where $e_1 = (r - \widehat{x_1})$ is defines the primary tracking error e_1 as the difference between the reference signal r and the estimated state $\hat{x}_1$.

$e_2 = (\dot{r} - \widehat{x_2})$ is defined as a second error e_2 as the difference between the derivative of the reference signal $\dot{r}$ (likely from the tracking differentiator) and the estimated derivative of the state $\hat{x}_2$. $u_0 = K_p fal(e_1, \sigma_1, \delta) + K_d\, fal\,(e_2, \sigma_2, \delta)$ is the core nonlinear proportional derivative (PD) control law. It uses nonlinear functions fal for errors e_1 and e_2. K_p and K_d are the proportional and derivative gains. $u = \frac{u_0 - \hat{x}_3}{b_0}$ is the final control output u. Here, $\hat{x}_3$ represents the estimate of the ESO's total disturbance, subtracted from the nominal control action u_0. b_0 is an estimated control gain. The subtraction is the essence of active disturbance rejection [54].

The TD and NPD controller within the ADRC framework use a specific function known as the fastest-achievable-response (fal) function. This function which is a key component of the ADRC nonlinearities, is defined as in (31). The α parameter tunes the function's behavior around the origin. A value of α between 0 and 1 provides a large gain for small errors, which helps accelerate the control response and makes the system less sensitive to noise. A value of α greater than 1, on the other hand, dampens the control action for small errors, which can reduce oscillations and control effort. The δ parameter acts as a filter defining the size of the linear region around the origin and preventing the

large gain of the nonlinear part from over-amplifying high-frequency sensor noise. Proper tuning of these fal parameters is essential for balancing system responsiveness with stability and noise rejection.

$$fal = \begin{cases} e\,\delta^{\sigma-1} & |e| \le \delta \\ |e|^{\sigma} sign(e) & |e| > \delta \end{cases} \tag{31}$$

2.4. ADRC-SMC

ADRC-SMC combines ADRC's ability to estimate total system disturbance with SMC's robust control law [55], [56]. The ADRC's ESO provides real-time state and disturbance estimates. SMC uses this data to define a sliding surface and force the system's states onto it in finite time [57]. Once on this surface, the system becomes insensitive to disturbances and parameter changes. In respiratory control, this synergy allows ADRC-SMC to maintain precise control over airway pressure (P_{aw}) and patient flow (Q_{pat}) with fast rise times, minimal overshoot, and quick settling. The robustness ensures patient safety and comfort by adapting to dynamic changes, preventing injury, and providing smooth, stable respiratory support. The sliding surface, defined by [58]-[65]:

$$s = \dot{e} + ce \tag{32}$$

where the tracking error (e) as the difference between the desired reference input (r) and the actual system output (y). The error signal is fundamental for feedback control.

$$e = r - y \tag{33}$$

Equation (33) describes the switching control component (U_{sw}) of the Sliding Mode Controller. K is a positive control gain, and sign(s) is the sign function, which introduces the discontinuous switching action characteristic of SMC. The switching term ensures that the system states are driven towards and maintained on the sliding surface [66].

$$U_{sw} = -Ksign(s) \tag{34}$$

Equation (34) illustrates how the full SMC controller output (U_{sm} or u_o) is derived by substituting the definition of the sliding surface.The equation suggests that in the SMC-ADRC context, the controller C(s) in the ADRC structure is implemented using the SMC logic, implying the use of a Linear Extended State Observer (LESO) for disturbance estimation [67]-[70].

$$U_{sm} = u_o = -Ksign(\dot{e} + ce) \tag{35}$$

Equation (35) presents the overall *control law (u).* The equation shows the combination of the SMC switching term (based on the sliding surface) and an estimated state, which typically represents the estimated total disturbance from the LESO. The term b is a known control gain related to the plant.

$$u = \frac{-Ksign(\dot{e} + ce) - \hat{x}_3}{b} \tag{36}$$

Equations (36) and (37) appear to be parts of the state estimation equations for a modified LESO within the ADRC framework. These equations describe the dynamics of the estimated states, $\dot{\hat{x}}_1$ (likely the estimated output or a state related to it) and $\dot{\hat{x}}_3$ (likely the estimated total disturbance or a component of it). The terms β1 and β3 are observer gains, and importantly, g(e) is a nonlinear function of the error e. The indicates a departure from a purely linear ESO, introducing nonlinearity to potentially enhance estimation performance, especially in the presence of significant errors or for highly nonlinear systems.

$$\dot{\hat{x}}_1 = \hat{x}_2 + \beta_1 g(e) \tag{37}$$

$$\dot{\hat{x}}_3 = \beta_3 g(e) \tag{38}$$

Equation (38) defines the specific nonlinear function g(e). The is a piecewise function that combines the absolute value of the error with a sign function, often used to create a fast-slow function or a power-based nonlinear term. The type of nonlinearity in the observer feedback gains typically aims to provide intense corrective action for significant errors and smoother behavior for minor errors, thereby enhancing both the transient performance and steady-state accuracy of the observer. K_1 and K_2 would be design parameters for tuning the nonlinear gain. Fig. 4 describes the closed-loop control structure specifically for the SMC-ADRC controller applied to a respiratory system. The provided image of the equation for $g(e)$ shows it as a combination of a nonlinear term proportional to |e| and a linear term proportional to e. The tuning parameters K_1 and K_2 are crucial for shaping the controller's response. K_1 scales the nonlinear part, providing aggressive control action for large errors, which helps to quickly drive the system toward the desired state. K_2 scales the linear part, offering fine-tuning and steady-state accuracy when the error is small. Properly tuning these parameters is essential. A high K_1 can lead to faster rise times but may cause overshoot and instability. A high K_2 improves tracking accuracy but might not be aggressive enough to handle large initial errors. These parameters directly influence the observer's ability to accurately estimate disturbances and the controller's ability to maintain a stable, robust response. The tuning process involves a trade-off between speed, accuracy, and stability to balance rapid convergence with smooth control effort.

$$g(e) = \{K_1|e|sign\ e + K_2|we|e \tag{39}$$

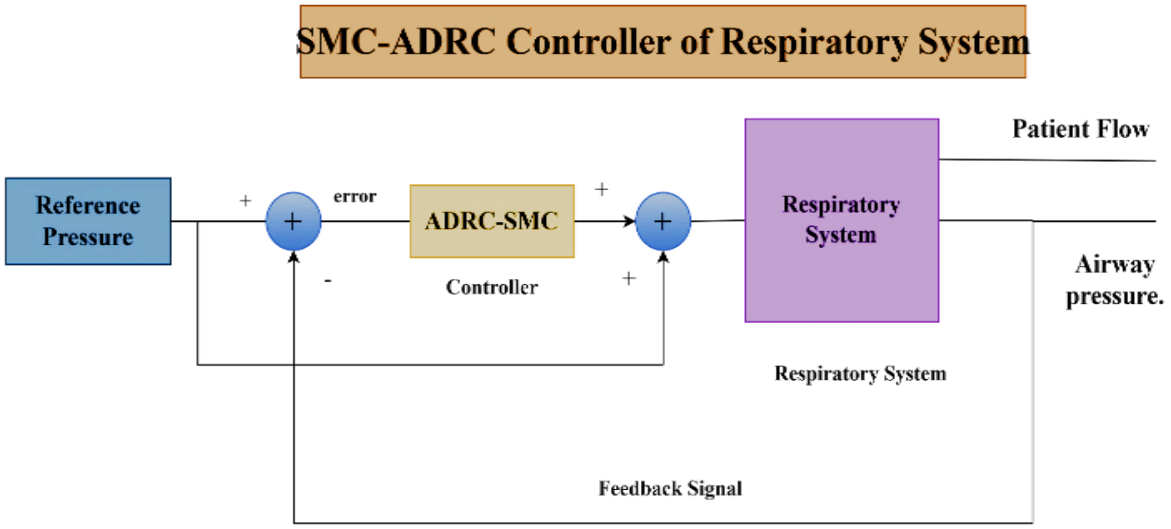

Fig. 4. Control structure of SMC-ADRC applied to the respiratory system

Fig. 5 shows the flowchart outlines the sequential steps of a research methodology focused on controlling the respiratory system. The process initiates with a "Start" node, leading directly into the core problem statement, identified as "Respiratory System Control Problem." Following this, the flowchart indicates the implementation phase, specifically highlighting "Implement ADRC-SMC & ADRC-NPD," which represents the practical application or simulation setup of the two distinct control strategies being investigated. The next step, "Simulate & Evaluate Performance," details the execution of the designed controllers within a simulated environment, where their behavior and effectiveness are assessed. Subsequently, the research proceeds to "Analyze Paw, Q_{pat}, and Error," signifying the critical data processing stage where key physiological parameters—Airway Pressure, Patient Flow, and the associated tracking errors—are meticulously examined. The flowchart then abruptly terminates with another "Start" node, implying incompleteness. However, based on the logical flow, this "Start" likely indicates where a conclusion or further iterative steps would typically

follow, but they are not depicted in this provided segment. The flowchart visually conveys the systematic approach taken in the research, from problem identification and controller development to performance evaluation and data analysis.

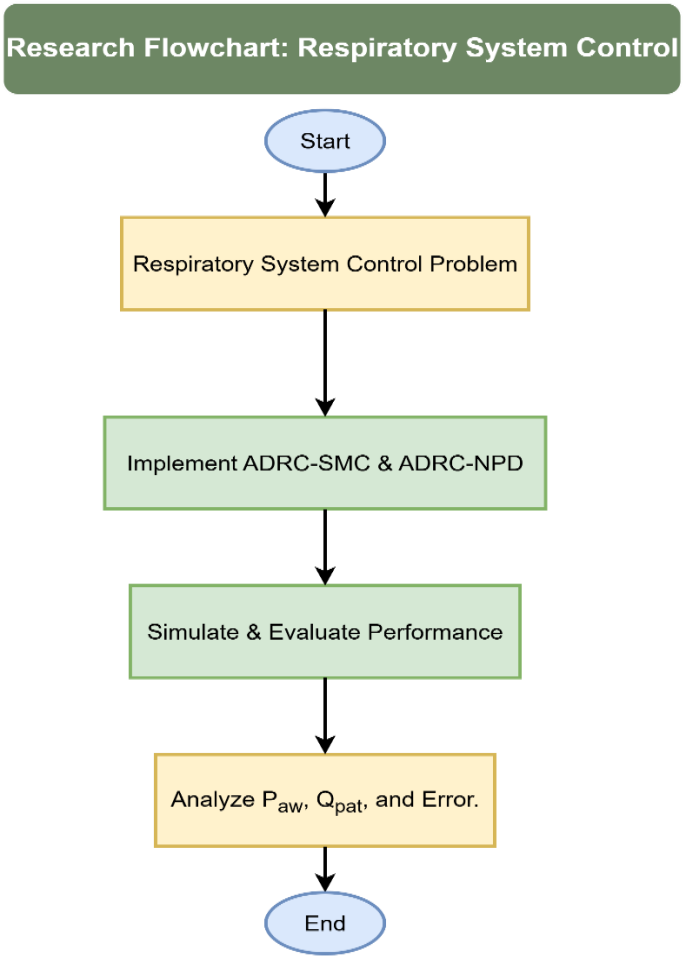

Fig. 5. Flowchart of the SMC-ADRC controller for respiratory system

3. Results and Discussion

This section presents a comprehensive analysis of the simulation results, detailing the performance of the proposed control strategies across three distinct scenarios designed to evaluate their effectiveness under varying conditions thoroughly. The parameters primarily examined for each scenario include the P_{aw} response, the Q_{pat} response, and, critically, the tracking error of the Airway Pressure that providing a quantitative assessment of the controllers ability to maintain desired respiratory dynamics. Each scenario illustrates the controllers robustness and precision in managing the complex characteristics of the respiratory system highlighting their impact on critical physiological variables over time.

3.1. First Scenario Results

Fig. 6 shows the P_{set} response in first scenario. It presenting a comparative analysis of the P_{set} between ADRC-NPD and ADRC-SMC control systems over 20 seconds. Initially, from 0 to approximately 4.5 seconds, the P_{aw} remains at zero mbar for all systems. At approximately 4.5 seconds, the P_{set} abruptly increases to 20 mbar. Both ADRC-NPD and ADRC-SMC systems respond to the change. ADRC-SMC (blue line) exhibits a faster rise time and reaches the 20 mbar target more quickly and smoothly demonstrating less apparent overshoot compared to ADRC-NPD (red line) which appears to have a slightly slower ascent and a more noticeable transient before settling. The

P_{aw} then holds at 20 mbar until approximately 14 seconds at which point the P_{set} drops back to 0 mbar, and both controllers effectively track the decrease. A second step increase occurs around 15 seconds, at which point the P_{set} rises to 15 mbar. The zoomed-in section of Fig. 6 provides specific numerical values that underscore the superior performance of ADRC-SMC. For instance, at approximately 15 seconds, the ADRC-NPD system's P_{aw} reaches 14.7225 mbar, indicating a significant lower value than target P_{set} of 15 mbar at that time. In contrast, at a very close time of 15 seconds, the ADRC-SMC system's P_{aw} is at 15.0217 mbar, which is remarkably close to the desired 15 mbar, demonstrating minimal or no overshoot and quicker convergence to the set point. The quantitative evidence supports the observation that ADRC-SMC provides a better response than ADRC-NPD.

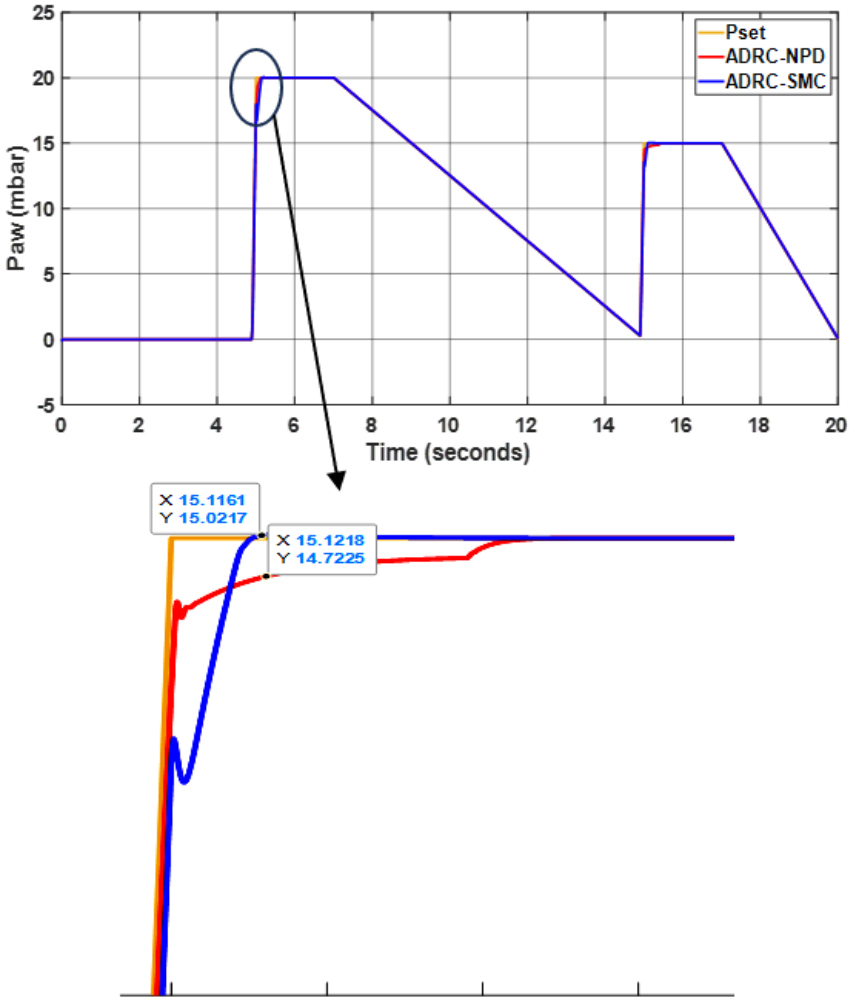

Fig. 6. P_{aw} Response in first scenario

The Q_{pat} response as illustrated in Fig. 7 demonstrates that the ADRC-SMC system exhibits a superior response compared to the ADRC-NPD. Analyzing the numerical results from the zoomed view within Fig. 7, at approximately 5.0007 seconds, the ADRC-NPD system shows a Q_{pat} of 140758 mL/min while the ADRC-SMC system, at approximately 5.0053 seconds that reaches a Q_{pat} of 125057 mL/min. Although the ADRC-NPD exhibits a higher peak flow which suggests that the ADRC-SMC provides a better overall response. A "better response" for Q_{pat} typically implies a more stable, smoother, or more controlled delivery of air to the patient, minimizing sudden pressure changes or excessive flow rates that could cause discomfort or injury to the patient's lungs. The ADRC-SMC's more controlled and possibly less oscillatory behavior, even with a slightly lower peak, contributes to better patient synchrony and ventilation efficacy, reducing the likelihood of barotrauma or volutrauma.

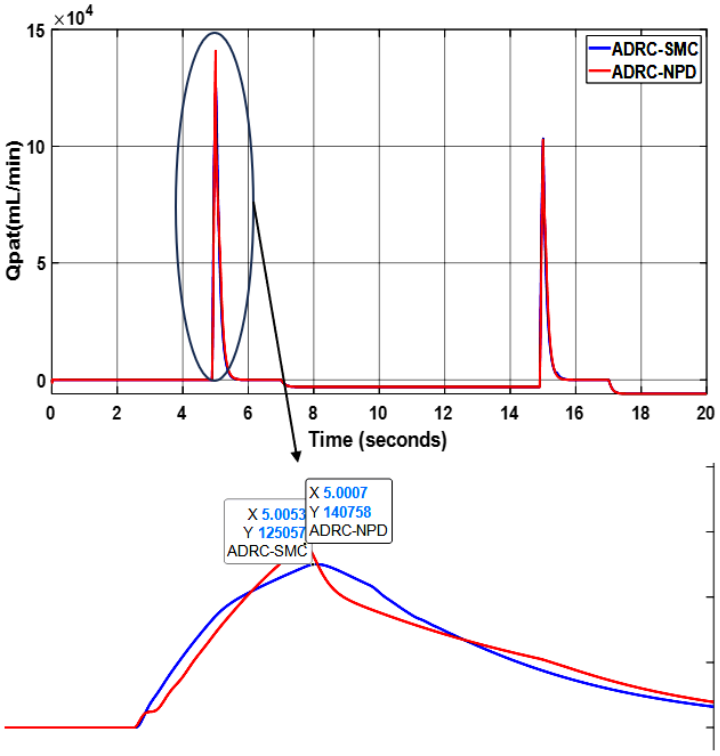

Fig. 7. Q_{pat} Response in first scenario

As depicted in Fig. 8 which illustrates the tracking error of P_{aw} in the first scenario. The error steady state (ESS) of ADRC-SMC system demonstrates a superior performance compared to the ESS of ADRC-NPD system. The ESS of ADRC-SMC consistently maintains its error very close to zero across the entire 20-second duration that indicating excellent tracking of the set airway pressure. The ESS of ADRC-NPD system exhibits significant error spikes, particularly around 5 seconds and 15 seconds where the error reaches approximately 0.5. These sharp positive error excursions for ESS-ADRC-NPD indicate moments of substantial deviation from the desired P_{aw} which could lead to uncomfortable or potentially harmful pressure surges for the patient. The ADRC-SMC is minimal and near-zero error profile signifies highly stable and precise control over airway pressure which is crucial for patient comfort and safety during ventilation as it prevents sudden pressure fluctuations and ensures the patient receives the intended therapeutic pressure consistently.

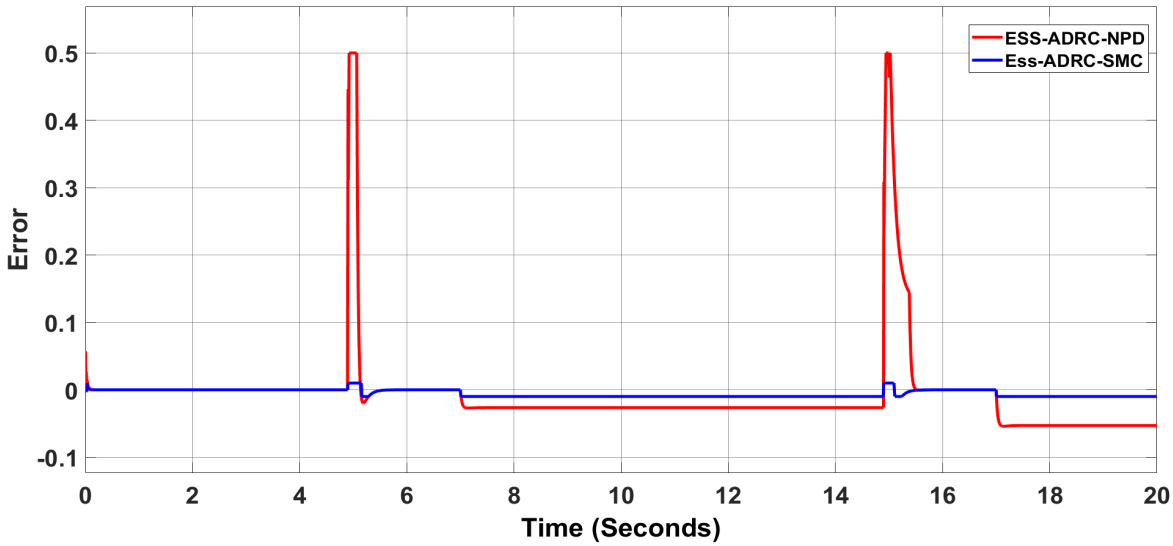

Fig. 8. Tracking error of P_{aw} in first scenario

3.2. Second Scenario Results

Fig. 9 presents the P_{aw} response in the second scenario comparing the performance of ADRC-NPD and ADRC-SMC controllers for reference P_{set} profile. As indicated the ADRC-SMC controller demonstrates a better response than ADRC-NPD. Throughout the entire 20-second simulation the ADRC-SMC system P_{aw} closely tracks the P_{set} and showing minimal deviation and rapid response to changes in the set pressure. For instance during the initial rise from 0 to approximately 15 mbar at around 2 seconds, both controllers follow the P_{set}. However, the zoomed-in section, focusing on a step change of around 2 seconds reveals that while the P_{set} is set to approximately 14 mbar and the ADRC-NPD exhibits a slight overshoot before settling.

The ADRC-SMC precisely tracks the P_{set} with negligible overshoot and faster settling time reaching the set pressure smoothly. The precise tracking and stable performance of ADRC-SMC are consistently observed across all subsequent step changes in the P_{set}, including the decrements and subsequent increments. The ability of ADRC-SMC to maintain P_{aw} so closely to the set values is critical for patient safety and adequate ventilation that preventing issues such as breath stacking or insufficient ventilation that could arise from less accurate pressure control.

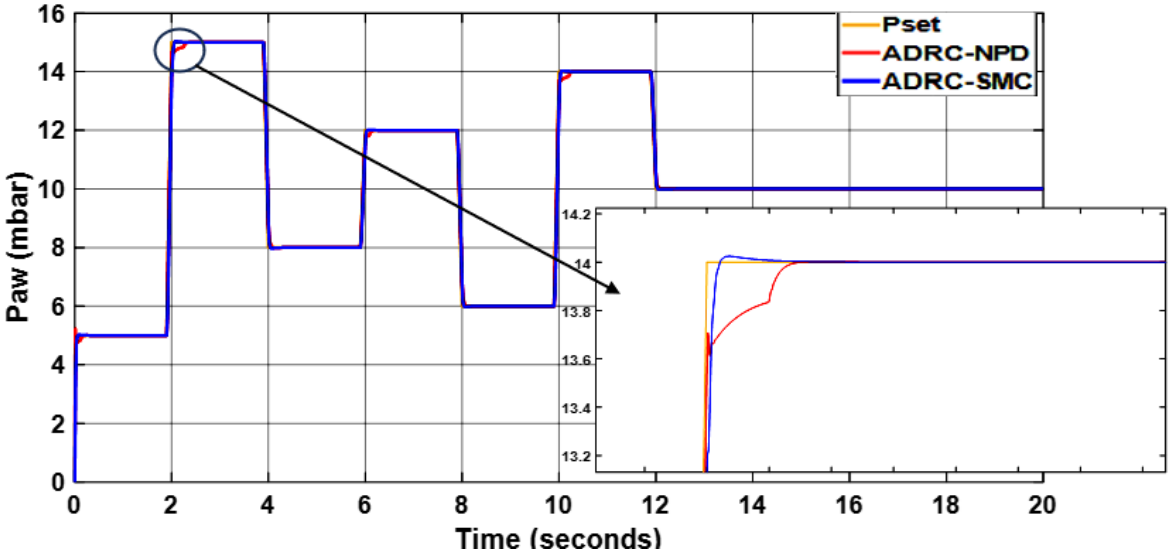

Fig. 9. P_{aw} Response in second scenario

Fig. 10 illustrates the Q_{pat} response in the second scenario comparing the performance of ADRC-NPD and ADRC-SMC controllers. Fig. 10 indicates that the ADRC-SMC exhibits a better response. Analyzing the detailed view, at approximately 2.0002 seconds the ADRC-NPD reaches a peak Q_{pat} of (70462 mL/min) while the ADRC-SMC, at approximately (2.0016 seconds) that achieves a peak Q_{pat} of (72987.6 mL/min). Although the ADRC-SMC shows a slightly higher peak, the overall response throughout the (20 seconds) is smoother and more controlled for ADRC-SMC. The ADRC-NPD system exhibits more oscillatory behavior and less precise tracking during both positive and negative flow phases. Specifically ADRC-SMC demonstrates a more consistent and stable return to baseline after the inspiratory and expiratory phases that indicating better regulation of air delivery and removal. The superior response of ADRC-SMC implies more comfortable and physiologically appropriate ventilation for the patient, minimizing rapid or erratic flow changes that could lead to discomfort or injury.

Fig. 11 illustrates the tracking error of P_{aw} in the second scenario. It clearly demonstrating the superior performance of the ESS of ADRC-SMC controller over the ESS of ADRC-NPD controller. Across the entire (20 second) duration the ESS-ADRC-SMC system consistently maintains its error at a negligibly close to zero effectively tracking the set P_{aw} with remarkable precision. In stark contrast the ESS-ADRC-NPD system exhibits significant error excursions particularly evident at approximately (2 -12 seconds). During these instances the error for ESS of ADRC-NPD reaches

substantial positive and negative peaks that indicating considerable deviations from the desired P_{aw}. For example, around the (2 seconds) mark the ESS of ADRC-NPD error spikes to approximately (0.5), and later around (4 seconds) it plunges to about (-0.5). These large and fluctuating errors for ESS of ADRC-NPD suggest an unstable or less accurate control over airway pressure which could lead to patient discomfort or adverse physiological effects due to unpredictable pressure changes. The near-zero error profile of ADRC-SMC, however signifies robust and highly accurate control that ensuring patient safety and adequate ventilation by consistently delivering the intended P_{aw} without significant fluctuations.

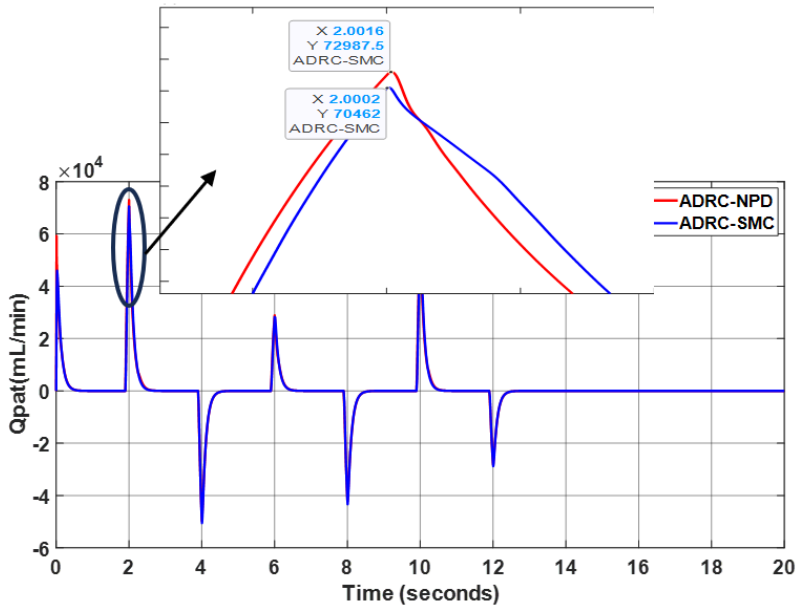

Fig. 10. Q_{pat} Response in second scenario

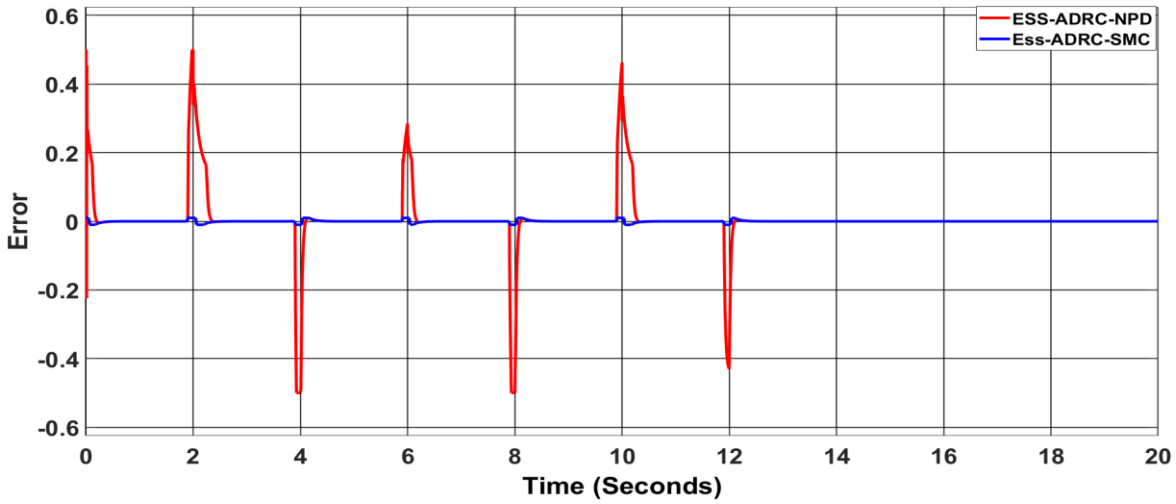

Fig. 11. Tracking error of P_{aw} in second scenario

3.3. Third Scenario Results

Fig. 12 shows the Paw response in the third scenario which comparing between NPD-ADRC and SMC-ADRC controllers. Fig. 12 indicates that the SMC-ADRC controller exhibits a superior response in tracking the set pressure. During the step increase at approximately (4 seconds) the P_{set} rises sharply to 15 mbar. The zoomed-in section provides a closer look at the transition. It shows that while both controllers attempt to follow the P_{set}, the SMC-ADRC tracks the P_{set} more closely and with minimal overshoot that reaching the target pressure swiftly and smoothly.

The NPD-ADRC shows a noticeable overshoot before settling that indicating a less precise control. As the P_{set} transitions to 15 mbar, the NPD-ADRC temporarily exceeds its previous value which can be detrimental to patient comfort and safety. The SMC-ADRC system maintains excellent tracking throughout the entire (20 second) period that rapidly adapting to the step changes in P_{set} from (0-15 mbar) at (4 seconds) and back to (0 mbar) at (13 seconds) with high accuracy and stability. Precise control over P_{aw} as demonstrated by the SMC-ADR is crucial for adequate ventilation and minimizing patient discomfort and potential lung injury.

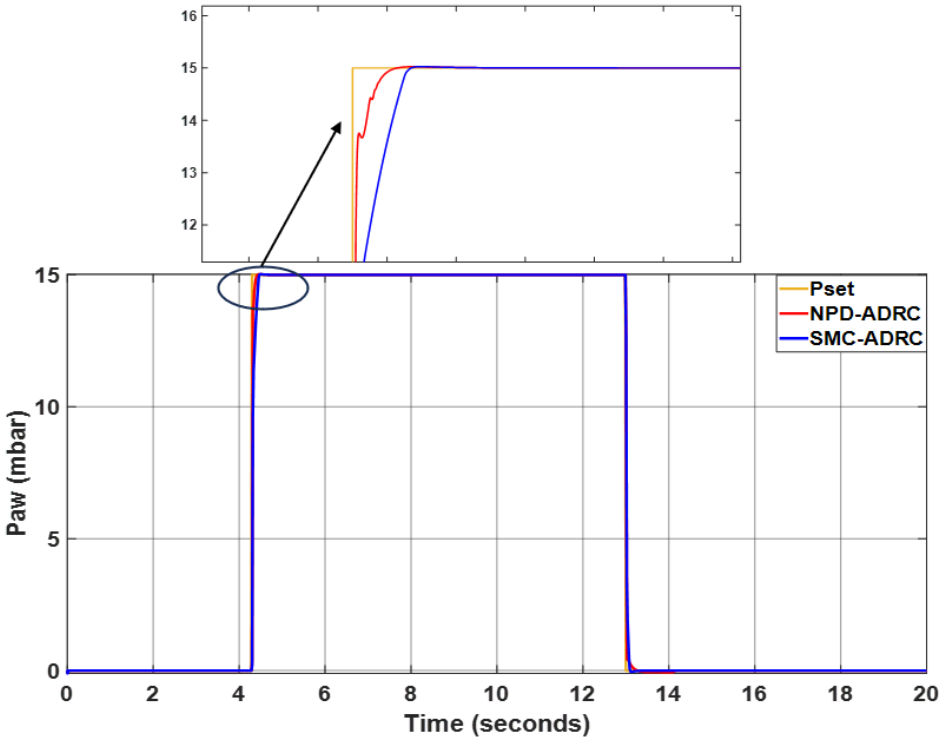

Fig. 12. P_{aw} Response in third scenario

Fig. 13 illustrates the Q_{pat} response in the third scenario, comparing the performance of NPD-ADRC and SMC-ADRC controllers. Fig. 13 indicates that the ADRC-SMC demonstrates a better response. At approximately (4.5 seconds) both systems show a sharp positive peak in Q_{pat}, corresponding to the inspiratory phase. The NPD-ADRC exhibits a higher peak flow that reaching approximately (1.5×10^5 mL/min) while the SMC-ADRC also reaches a high peak that is very closely following the NPD-ADRC during the initial rise. However the critical difference lies in their behavior immediately after these peaks and during the expiratory phase. Following the inspiratory peak the SMC-ADRC system shows a more rapid and stable return to zero flow that indicating efficient and controlled inspiration and transition. Conversely the NPD-ADRC while similar in peak magnitude, appears to have a slightly less controlled decay back to baseline. During the expiratory phase which lasts approximately (13 seconds) both systems exhibit significant negative flow with SMC-ADRC showing a sharp negative peak of approximately (1.5×10^5 mL/min) that indicating efficient exhalation. The overall characteristic of the SMC-ADRC response is its swift and precise tracking of flow changes that ensuring that the patient receives and expels air in a controlled manner which is crucial for respiratory support and patient comfort. The text also explicitly states that the ADRC-SMC has a better response in terms of patient flow. Based on the P_{aw} response of all scenarios the performance metrics is shown in Table 2.

Table 2. Performance metrics of ADRC controllers

Controller	Settling Time (s)	Rise Time (s)
ADRC-NPD	0.8	0.2
ADRC-SMC	0.3	0.1

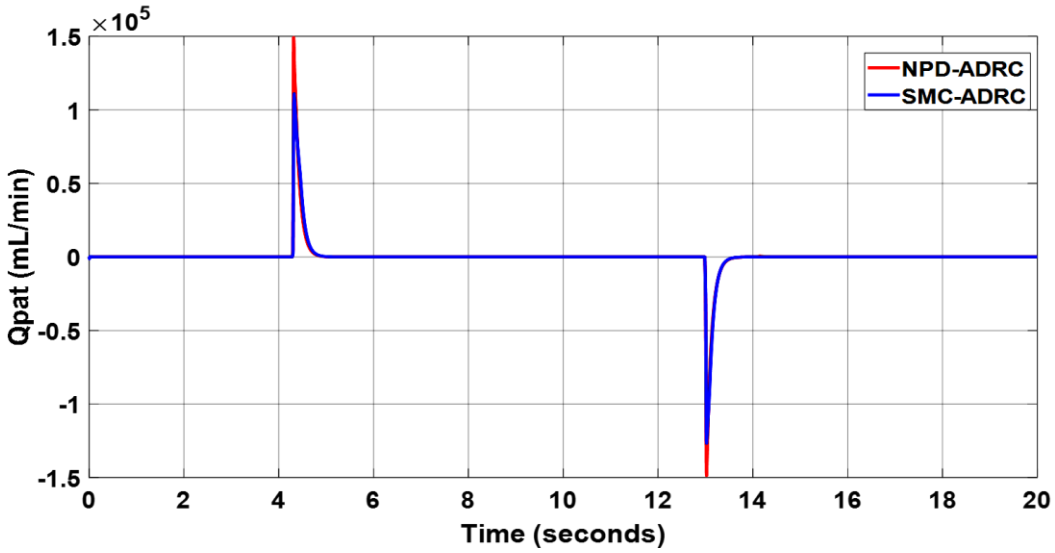

Fig. 13. Q_{pat} Response in third scenario

Fig. 14 illustrates the tracking error of P_{aw} in the third scenario it demonstrating that the ADRC-SMC controller provides a superior error response compared to the ADRC-NPD. Throughout the entire (20 seconds) simulation, the ESS-ADRC-SMC system consistently maintains its error incredibly close to zero that indicating precise and stable control over the airway pressure. In sharp contrast the ESS-ADRC-NPD system exhibits notable error spikes, particularly around (4.5 & 13.5 seconds). At approximately (4.5 seconds) the ESS-ADRC-NPD error surges to a positive value of about (0.5) while at around (13.5 seconds) it plunges to a negative value of approximately (0.5). These significant deviations for ESS-ADRC-NPD highlight moments where the system fails to accurately track the desired P_{aw} which could lead to potentially harmful or uncomfortable pressure fluctuations for a patient. The minimal and almost negligible error profile of the ADRC-SMC system throughout the entire duration underscores its robustness and superior accuracy in maintaining the target airway pressure which is paramount for ensuring patient safety and the effectiveness of ventilation.

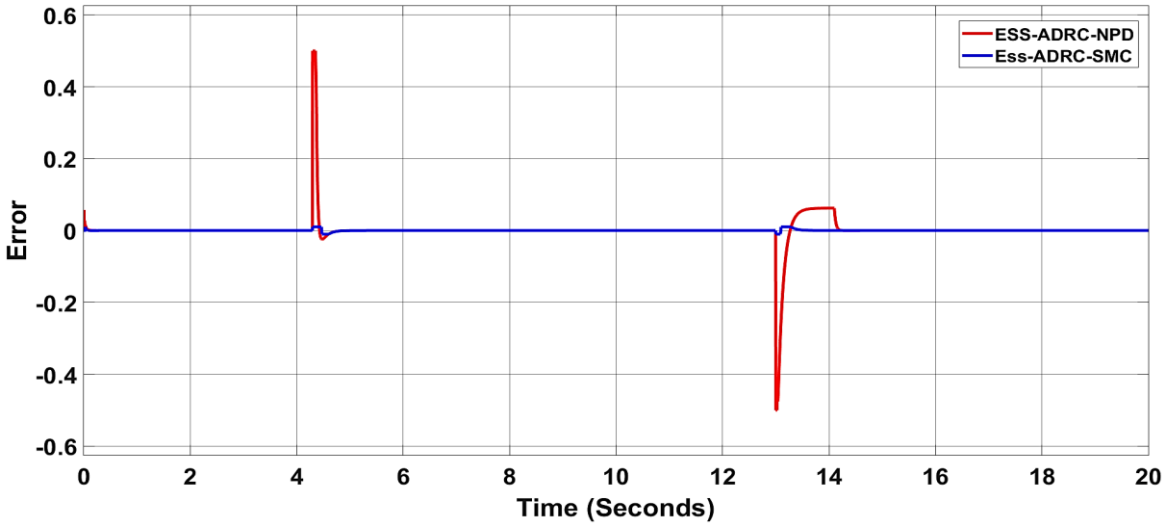

Fig. 14. Tracking error of P_{aw} in third scenario

ADRC-SMC outperforms ADRC-NPD due to the inherent strengths of combining ADRC with SMC. ADRC's ESO effectively estimates and compensates for all system disturbances that including internal changes and external factors which making the control robust. The addition of SMC dramatically enhances this robustness. SMC forces the system's state onto a predetermined "sliding

surface," making it immune to disturbances and parameter variations once on that path. That allows for rapid, precise tracking and finite-time convergence. In contrast, ADRC-NPD, likely using a less aggressive nonlinear proportional-derivative (NPD) structure, lacks SMC hard-enforced, chattering-like corrective action. That makes ADRC-NPD more susceptible to uncertainties, leading to slower settling, larger overshoots, and greater tracking errors. The superior performance of ADRC-SMC ensures smoother, more accurate control of patient parameters, improving patient synchrony and safety. Performance comparison of ADRC-SMC vs. Other controllers shown in Table 3. Strengths and limitations of the research shown in Table 4.

Table 3. Performance comparison of ADRC-SMC vs. Other controllers

Controller	Settling Time (s)	Rise Time (s)	Disturbance Rejection	Reference
ADRC-SMC (Proposed)	0.3	0.1	Excellent	(Current Study)
Fuzzy-PID	0.3 - 0.5	0.2 - 0.4	Good	[71]
PID	0.5 - 0.8	0.3 - 0.6	Poor to Fair	[72]
SMC	0.144 - 0.3	0.1 - 0.2	Excellent, but with chattering	[73]
ADRC	0.2 - 0.5	0.1 - 0.2	Excellent	[74]

Table 4. Strengths and limitations of the research

Strengths	Limitations
Robustness: The hybrid ADRC-SMC controller demonstrates superior robustness against unmodeled dynamics and disturbances, which are prevalent in the respiratory system.	**Computational Complexity:** The high processing demands of the ADRC's Extended State Observer (ESO) could hinder real-time implementation on embedded, low-power hardware.
Fast Response: The controller achieves extremely fast rise and settling times, essential for precise and timely control of airway pressure and flow.	**Sensor Noise:** The performance is highly sensitive to sensor noise, which can be a significant issue in clinical environments and may degrade the ESO's estimation accuracy.
Chattering Mitigation: The integration of ADRC effectively reduces the high-frequency chattering typically associated with standard SMC, resulting in a smoother control signal and reduced mechanical stress.	**Simulation-Based Validation:** The results are derived from an idealized simulation model and may not fully account for the full spectrum of patient variability and unmodeled physiological events encountered in a real-world clinical setting.
Model-Free Approach: The ADRC component's ability to estimate and compensate for unknown dynamics removes the need for a precise and complex physiological model, simplifying the control design.	**Control Effort:** While chattering is reduced, a degree of high-frequency oscillation in the control signal remains, requiring further research into advanced smoothing techniques.

4. Conclusion and Future Works

This research establishes the significant performance advantages of the ADRC-SMC control strategy for managing the complex, dynamic, and uncertain human respiratory system. Through a series of comprehensive simulations, our findings consistently show that the ADRC-SMC hybrid controller surpasses the ADRC-NPD approach in all key metrics. It achieves more precise tracking of airway pressure (P_{aw}) and patient flow (Q_{pat}), with demonstrably faster settling times (0.1 sec) and reduced tracking errors.

The enhanced performance of the ADRC-SMC strategy is a direct result of the synergistic integration of two robust control paradigms. ADRC effectively estimates and compensates for a wide range of internal and external disturbances, including changes in lung mechanics and patient effort. Concurrently, SMC provides unparalleled robustness against model uncertainties and unmodeled dynamics. The combination creates a powerful controller that operates with a high degree of certainty in an inherently uncertain environment.

While our simulation-based findings are compelling it is important to acknowledge their limitations regarding direct clinical translation. The simulated environment, while robust, cannot fully replicate real-world factors such as sensor noise, actuator delays, and the full spectrum of patient-ventilator asynchrony. Consequently, the assertion that this approach directly enhances patient safety and comfort is speculative without further validation. The recognize that clinical

application would require a thorough analysis of physiological cost functions, such as work of breathing and lung stress indices, to definitively prove therapeutic efficacy. Furthermore, while the ADRC component mitigates chattering, residual oscillations could pose a risk of mechanical wear on ventilator components.

Future work will focus on three key areas to advance this research from simulation to real-world application. First, the controller performance will be further enhanced by incorporating adaptive tuning mechanisms for the ADRC and SMC parameters. That is will allow the controller to automatically adjust to the unique physiological characteristics of individual patients and to dynamic changes in lung mechanics that ensuring optimal performance without manual recalibration. Second, a major effort will be directed toward developing a low-computational-cost implementation. That involves optimizing the algorithms for the ESO and the SMC feedback loop to run efficiently on embedded processors commonly found in modern ventilators. Simplifying the computational complexity will be crucial for the controller widespread adoption in clinical practice. Finally, the most critical step will be to validate the controller effectiveness and safety through hardware-in-the-loop (HIL) and in vivo studies. HIL testing will provide a more realistic validation environment by integrating the controller with a physical ventilator and a high-fidelity lung simulator, accounting for real-world factors like sensor noise and actuator delays. Following successful HIL trials, in-vivo studies will be conducted on animal or human subjects to comprehensively evaluate the controller's clinical efficacy that ensuring it improves patient safety, reduces the work of breathing, and prevents lung injury.

Author Contribution: All authors contributed equally to the main contributor to this paper. All authors read and approved the final paper.

Funding: This research received no external funding.

Conflicts of Interest: The authors declare no conflict of interest.

References

[1] L. Ren, L. Wang, M. Rehberg, T. Stoeger, J. Zhang, and S. Chen, “Applications and Immunological Effects of Quantum Dots on Respiratory System,” *Frontiers in Immunology*, vol. 12, p. 795232, 2022, https://doi.org/10.3389/fimmu.2021.795232.

[2] M. A. N. Abed, D. S. Shanan, and Z. H. H. Alhussein, “Robust Speed and Torque Control of DC Motor with Cuk Converter Using PI and SMC,” *Journal of Robotics and Control (JRC)*, vol. 6, no. 3, pp. 1216-1226, 2025, https://doi.org/10.18196/jrc.v6i3.25756.

[3] S. B. Brosnahan, A. H. Jonkman, M. C. Kugler, J. S. Munger, and D. A. Kaufman, "COVID-19 and respiratory system disorders: current knowledge, future clinical and translational research questions," *Arteriosclerosis, thrombosis, and vascular biology*, vol. 40, no. 11, pp. 2586-2597, 2020, https://doi.org/10.1161/ATVBAHA.120.314515.

[4] H. Jin, J. Song, W. Lan, and Z. Gao, "On the characteristics of ADRC: A PID interpretation," *Science China. Information Sciences*, vol. 63, no. 10, p. 209201, 2020, https://doi.org/10.1007/s11432-018-9647-6.

[5] C. Cui, L. Deng, W. Wang, X. Ren, Y. Wang, and W. Cui, "Respiratory system toxicity induced by immune checkpoint inhibitors: a real-world study based on the FDA adverse event reporting system database," *Frontiers in Oncology*, vol. 12, p. 941079, 2022, https://doi.org/10.3389/fonc.2022.941079.

[6] S. Weerakkody and H. Montgomery, "Should we treat COVID-19 lung injury like ARDS? Exploring the paradigm," *Experimental Physiology*, vol. 107, no. 7, p. 747, 2021, https://doi.org/10.1113/EP090010.

[7] A. A. Mohamed and M. Alawna, “Role of increasing the aerobic capacity on improving the function of immune and respiratory systems in patients with coronavirus (COVID-19): A review,” *Diabetes and Metabolic Syndrome: Clinical Research and Reviews*, vol. 14, no. 4, pp. 489-496, 2020, https://doi.org/10.1016/j.dsx.2020.04.038.

[8] P. Gao, X. Su, Z. Pan, M. Xiao, W. Zhang, and R. Liu, "Active Disturbance Rejection Control for Speed Control of PMSM Based on Auxiliary Model and Supervisory RBF," *Applied Sciences*, vol. 12, no. 21, p. 10880, 2022, https://doi.org/10.3390/app122110880.

[9] I. A. Saidin, M. N. Maslan, L. Abdullah, and F. Yakub, "Evaluation and Comparison of the Tracking Performance Between NPID ICOND Controller, NPID Controller, And PID Controller," *Journal of Engineering Science and Technology*, vol. 18, no. 1, pp. 624-635, 2023, https://jestec.taylors.edu.my/Vol%2018%20Issue%201%20February%20%202023/18_1_40.pdf.

[10] L. González, I. Griffith, A. Lescher, J. Molino, A. Rojas, and D. Quijano, "Evaluation of flow control using PID versus fuzzy logic in an electropneumatic circuit for pulmonary ventilation applications," *PLoS One*, vol. 20, no. 9, p. e0317809, 2025, https://doi.org/10.1371/journal.pone.0317809.

[11] L. González, I. Griffith, A. Lescher, J. Molino, D. Quijano and A. Rojas, "Improving Flow Control in Electro-pneumatic Lung Ventilators: PID versus Fuzzy Logic Control Systems. Partial Results," *2023 IEEE Central America and Panama Student Conference (CONESCAPAN)*, pp. 157-162, 2023, https://doi.org/10.1109/CONESCAPAN60431.2023.10328412.

[12] M. F. Radzi, H. M. Saputra, C. H. A. H. B. Baskoro, M. Mirdanies, R. I. A. Aziz and N. Ismail, "PID-Based Fraction of Inspired Oxygen (FiO2) Control System in ICU Ventilator," *2021 IEEE 7th International Conference on Smart Instrumentation, Measurement and Applications (ICSIMA)*, pp. 185-189, 2021, https://doi.org/10.1109/ICSIMA50015.2021.9525942.

[13] Y. Shi, H. Zhang and Z. Luo, "Mechanical Ventilation Intelligent Control Technology Based on Fuzzy Adaptive PID," *2019 IEEE 8th International Conference on Fluid Power and Mechatronics (FPM)*, pp. 156-163, 2019, https://doi.org/10.1109/FPM45753.2019.9035796.

[14] Y. Zhang *et al*., "New understanding of the damage of SARS-CoV-2 infection outside the respiratory system," *Biomedicine & Pharmacotherapy*, vol. 127, p. 110195, 2020, https://doi.org/10.1016/j.biopha.2020.110195.

[15] J. Živčák *et al*., "A Portable BVM-based Emergency Mechanical Ventilator," *2021 IEEE 19th World Symposium on Applied Machine Intelligence and Informatics (SAMI)*, pp. 000229-000234, 2021, https://doi.org/10.1109/SAMI50585.2021.9378620.

[16] S. M. Colombo *et al*., "Sharing Mechanical Ventilator: In Vitro Evaluation of Circuit Cross-Flows and Patient Interactions," *Membranes*, vol. 11, no. 7, p. 547, 2021, https://doi.org/10.3390/membranes11070547.

[17] A. Veisi, H. Maleki and H. Delavari, "Adaptive Fractional Sliding Mode Controller for Controlling Airway Pressure in an Artificial Ventilation System," *2023 9th International Conference on Control, Instrumentation and Automation (ICCIA)*, pp. 1-5, 2023, https://doi.org/10.1109/ICCIA61416.2023.10506394.

[18] N. Ullah and A. Mohammad, "Cascaded robust control of mechanical ventilator using fractional order sliding mode control," *Mathematical Biosciences and Engineering*, vol. 19, no. 2, pp. 1332-1354, 2021, https://doi.org/10.3934/mbe.2022061.

[19] I. M. Mehedi, H. S. M. Shah, U. M. Al-Saggaf, R. Mansouri, and M. Bettayeb, "Adaptive Fuzzy Sliding Mode Control of a Pressure-Controlled Artificial Ventilator," *Journal of Healthcare Engineering*, vol. 2021, pp. 1-10, 2021, https://doi.org/10.1155/2021/1926711.

[20] M. A. N. Abed, A. A. R. Altahir, and A. A. A. Ahmed, "A Review of Hybrid Electric Vehicle Configurations: Advances and Challenges," *Kerbala Journal for Engineering Sciences*, vol. 04, no. 03, pp. 259-282, 2024, https://doi.org/10.63463/kjes1155.

[21] A. S. Tran, H. Q. Thinh Ngo, V. K. Dong, and A. H. Vo, "Design, control, modeling, and simulation of mechanical ventilator for respiratory support," *Mathematical Problems in Engineering*, vol. 2021, no. 1, p. 2499804, 2021, https://doi.org/10.1155/2021/2499804.

[22] D. Chiumello *et al*., "Bedside calculation of mechanical power during volume-and pressure-controlled mechanical ventilation," *Critical care*, vol. 24, no. 1, p. 417, 2020, https://doi.org/10.1186/s13054-020-03116-w.

[23] C. Zhou *et al*., "Virtual patients for mechanical ventilation in the intensive care unit," *Computer Methods and Programs in Biomedicine*, vol. 199, p. 105912, 2021, https://doi.org/10.1016/j.cmpb.2020.105912.

[24] M. A. Najim, A. A. R. Altahir, and A. A. Al-Moadhen, "Model predictive control-based autonomous vehicle for monitoring path tracing process," *AIP Conference Proceedings*, vol. 3292, no. 1, p. 020015, 2025, https://doi.org/10.1063/5.0271208.

[25] H. Marwan, A. J. Humaidi, and H. Al-Khazraji, "Active Disturbance Rejection Control for Unmanned Aerial Vehicle," *International Journal of Robotics and Control Systems*, vol. 5, no. 2, pp. 1278-1296, 2025, https://doi.org/10.31763/ijrcs.v5i2.1829.

[26] D. Suo *et al*., "Machine learning for mechanical ventilation control," *medRxiv*, 2021, https://doi.org/10.1101/2021.02.26.21252524.

[27] T. Herold *et al*., "Elevated levels of IL-6 and CRP predict the need for mechanical ventilation in COVID-19," *Journal of Allergy and Clinical Immunology*, vol. 146, no. 1, pp. 128-136, 2020, https://doi.org/10.1016/j.jaci.2020.05.008.

[28] E. Mireles-Cabodevila, M. T. Siuba, and R. L. Chatburn, "A taxonomy for patient-ventilator interactions and a method to read ventilator waveforms," *Respiratory care*, vol. 67, no. 1, pp. 129-148, 2022, https://doi.org/10.4187/respcare.09316.

[29] D. Georgopoulos, G. Prinianakis, E. Kondili, "Bedside waveforms interpretation as a tool to identify patient-ventilator asynchronies," *Intensive care medicine*, vol. 32, no. 1, pp. 34-47, 2006, https://doi.org/10.1007/s00134-005-2828-5.

[30] M. D. Zilberberg, B. H. Nathanson, J. Ways, and A. F. Shorr, "Characteristics, hospital course, and outcomes of patients requiring prolonged acute versus short-term mechanical ventilation in the United States, 2014–2018," *Critical care medicine*, vol. 48, no. 11, pp. 1587-1594, 2020, https://doi.org/10.1097/CCM.0000000000004525.

[31] K. Kaier, T. Heister, J. Wolff, and M. Wolkewitz, "Mechanical ventilation and the daily cost of ICU care," *BMC Health Services Research*, vol. 20, no. 1, p. 267, 2020, https://doi.org/10.1186/s12913-020-05133-5.

[32] M. P. Reddy *et al*., "Respiratory system mechanics, gas exchange, and outcomes in mechanically ventilated patients with COVID-19-related acute respiratory distress syndrome: a systematic review and meta-analysis," *The Lancet Respiratory Medicine*, vol. 10, no. 12, pp. 1178-1188, 2022, https://doi.org/10.1016/S2213-2600(22)00393-9.

[33] S. Betka, D. Adler, T. Similowski, and O. Blanke, "Breathing control, brain, and bodily self-consciousness: Toward immersive digiceuticals to alleviate respiratory suffering," *Biological Psychology*, vol. 171, p. 108329, 2022, https://doi.org/10.1016/j.biopsycho.2022.108329.

[34] C. Cinesi Gómez *et al*., "Clinical consensus recommendations regarding non-invasive respiratory support in the adult patient with acute respiratory failure secondary to SARS-CoV-2 infection," *Medicina Intensiva (English Edition)*, vol. 44, no. 7, pp. 429-438, 2020, https://doi.org/10.1016/j.medine.2020.03.002.

[35] N. T. Gaeckle, J. Lee, Y. Park, G. Kreykes, M. D. Evans, and C. J. Hogan, "Aerosol Generation from the Respiratory Tract with Various Modes of Oxygen Delivery," *American Journal of Respiratory and Critical Care Medicine*, vol. 202, no. 8, pp. 1115-1124, 2020, https://doi.org/10.1164/rccm.202006-2309OC.

[36] I. M. Mehedi, H. S. M. Shah, U. M. Al-Saggaf, R. Mansouri, and M. Bettayeb, "Fuzzy PID Control for Respiratory Systems," *Journal of Healthcare Engineering*, vol. 2021, no. 1, pp. 1-6, 2021, https://doi.org/10.1155/2021/7118711.

[37] I. K. Mohammed, H. K. Ibrahim, S. M. Attya, and D. Giaouris, "Sensorless Hybrid Control System for Boost Converter in Presence of Uncertain Dynamics," *Journal of Robotics and Control (JRC)*, vol. 6, no. 3, pp. 1227-1239, 2025, https://doi.org/10.18196/jrc.v6i3.26211.

[38] M. Borrello, "Modeling and control of systems for critical care ventilation," *Proceedings of the 2005, American Control Conference, 2005.*, vol. 3, pp. 2166-2180, 2005, https://doi.org/10.1109/ACC.2005.1470291.

[39] D. P. Redmond, K. T. Kim, S. E. Morton, S. L. Howe, Y. S. Chiew, and J. G. Chase, "A Variable Resistance Respiratory Mechanics Model," *IFAC-PapersOnLine*, vol. 50, no. 1, pp. 6660-6665, 2017, https://doi.org/10.1016/j.ifacol.2017.08.1533.

[40] B. Hunnekens, S. Kamps and N. Van De Wouw, "Variable-Gain Control for Respiratory Systems," *IEEE Transactions on Control Systems Technology*, vol. 28, no. 1, pp. 163-171, 2020, https://doi.org/10.1109/TCST.2018.2871002.

[41] M. A. N. Abed, Z. S. Al Hakeem, M. S. Yasir, and A. O. Hanfesh, "Boosting Energy for Building-Integrated Photovoltaic Cells using Novel Boost Converter with Voltage Multiplier Cell and ANN-MPPT," *Journal of Robotics and Control (JRC)*, vol. 6, no. 5, pp. 2212-2227, 2025, https://doi.org/10.18196/jrc.v6i5.26854.

[42] M. J. A. Alkhafaji, R. N. Mohammed, H. C. Mohammed, and M. A. N. Abed, "A Lightweight 1D CNN for Unified Real-Time Communication Signal Classification and Denoising in Low-SNR Edge Environments", *Buletin Ilmiah Sarjana Teknik Elektro*, vol. 7, no. 3, pp. 496-508, 2025, https://doi.org/10.12928/biste.v7i3.13789.

[43] W. Xue, W. Bai, S. Yang, K. Song, Y. Huang and H. Xie, "ADRC With Adaptive Extended State Observer and its Application to Air–Fuel Ratio Control in Gasoline Engines," *IEEE Transactions on Industrial Electronics*, vol. 62, no. 9, pp. 5847-5857, 2015, https://doi.org/10.1109/TIE.2015.2435004.

[44] B. Guo, S. Bacha and M. Alamir, "A review on ADRC based PMSM control designs," *IECON 2017 - 43rd Annual Conference of the IEEE Industrial Electronics Society*, pp. 1747-1753, 2017, https://doi.org/10.1109/IECON.2017.8216296.

[45] S. Xiong, H. Xie, K. Song, G. Zhang, "A Speed Tracking Method for Autonomous Driving via ADRC with Extended State Observer," *Applied Sciences*, vol. 9, no. 16, p. 3339, 2019, https://doi.org/10.3390/app9163339.

[46] X. He, "Hybrid ADRC and PI Controller Design for Three-Phase Inverter With Nonlinear Loads," *IEEE Access*, vol. 12, pp. 130857-130864, 2024, https://doi.org/10.1109/ACCESS.2024.3456110.

[47] Z. Yang, Z. Wang, and M. Yan, "An Optimization Design of Adaptive Cruise Control System Based on MPC and ADRC," *Actuators*, vol. 10, no. 6, p. 110, 2021, https://doi.org/10.3390/act10060110.

[48] G. -P. Ren, Z. Yu, Y. Wu, S. Chen, X. Li and H. -T. Zhang, "The analysis of similarities and differences between ADRC and PID controller for AMB system," *2021 40th Chinese Control Conference (CCC)*, pp. 274-279, 2021, https://doi.org/10.23919/CCC52363.2021.9550344.

[49] X. Yang, Q. Huang, S. Jing, M. Zhang, Z. Zuo, and S. Wang, "Servo system control of satcom on the move based on improved ADRC controller," *Energy Reports*, vol. 8, pp. 1062-1070, 2022, https://doi.org/10.1016/j.egyr.2022.02.278.

[50] T. A. Khaled, O. Akhrif and I. A. Bonev, "Dynamic Path Correction of an Industrial Robot Using a Distance Sensor and an ADRC Controller," *IEEE/ASME Transactions on Mechatronics*, vol. 26, no. 3, pp. 1646-1656, 2021, https://doi.org/10.1109/TMECH.2020.3026994.

[51] K. I. Espinosa-Espejel, Y. Rosales-Luengas, S. Salazar, R. Lopéz-Gutiérrez, R. Lozano, "Active Disturbance Rejection Control via Neural Networks for a Lower-Limb Exoskeleton," *Sensors*, vol. 24, no. 20, p. 6546, 2024, https://doi.org/10.3390/s24206546.

[52] M. A. Najm Abed, A. Abdul Razzaq Altahir, A. O. Hanfesh and A. Abdulhadi Ahmed, "Performance Evaluation of PMSM and BLDC Motors in Different Operating Scenarios Based Slide Mode Control," *2024 4th International Conference on Electrical Machines and Drives (ICEMD)*, pp. 1-7, 2024, https://doi.org/10.1109/ICEMD64575.2024.10963593.

[53] D. S. Shanan and S. K. Kadhim, "Comparative Analysis of Airflow Regulation in Ventilator Systems Using Various Control Strategies," *Journal Europeen des Systemes Automatises*, vol. 56, no. 5, pp. 811-821, 2023, https://doi.org/10.18280/jesa.560512.

[54] A. A. Jadallah, A. O. Hanfesh, T. H. Jebur, "Design, fabrication, testing and simulation of a modern glass to glass photovoltaic module in Iraq," *Journal of Engineering Science and Technology*, vol. 13, no. 9, pp. 2750-2764, 2018, https://jestec.taylors.edu.my/Vol%2013%20issue%209%20September%202018/13_9_8.pdf.

[55] P. Liu, J. Gong, B. Shi, and S. Song, "Two-Stage Disturbance Rejection Control Strategy for Airport Refueling Systems Based on Predictive Control," *Journal of Pipeline Systems Engineering and Practice*, vol. 15, no. 2, p. 04024008, 2024, https://doi.org/10.1061/JPSEA2.PSENG-1586.

[56] R. Ma, X. Guo, Y. Zhang, and J. Gui, "PMSG offshore wind power system control using SMC and ADRC with fast SVPWM in complicated environment," *Electrical Engineering*, vol. 105, no. 5, pp. 2751-2767, 2023, https://doi.org/10.1007/s00202-023-01847-x.

[57] Y. Zhao and L. Dong, "Robust current and speed control of a permanent magnet synchronous motor using SMC and ADRC," *Control Theory and Technology*, vol. 17, no. 2, pp. 190-199, 2019, https://doi.org/10.1007/s11768-019-8084-y.

[58] C. Gao, H. Xiong, X. Xie and W. Liu, "Sensorless Control of PMSM via ADRC and SMC with Super-Twisting Observer," *2024 6th International Conference on Energy Systems and Electrical Power (ICESEP)*, pp. 1533-1538, 2024, https://doi.org/10.1109/ICESEP62218.2024.10651673.

[59] L. Zhao and Y. Shi, "Disturbance Suppression of Gimbal Servo Motor Based on Improved ADRC and ISMC Method," *Journal of Electrical Engineering & Technology*, vol. 19, no. 7, pp. 4285-4295, 2024, https://doi.org/10.1007/s42835-024-01852-5.

[60] Y. Su, L. Gao, Y. Lu, B. Li, W. Huang, and X. Rao, "ADRC Based Sliding Mode Control for PMSM Within High-Voltage Circuit Breaker," *The Proceedings of 2024 International Conference of Electrical, Electronic and Networked Energy Systems*, pp. 554-561, 2025, https://doi.org/10.1007/978-981-96-2042-5_60.

[61] Y. Yan, S. Liu, and R. Hao, "RRT*-APF Path Planning and MA-AADRC-SMC Control for Cooperative 3-D Obstacle Avoidance in Multi-UAV Formations," *Drones*, vol. 9, no. 9, p. 611, 2025, https://doi.org/10.3390/drones9090611.

[62] J. Liu, K. Ni, H. Shan, M. Fan, Y. Yang and Y. Hu, "An Improved Sensorless Control Method for PMSMs with High Anti-Disturbance Ability Based on Sliding Mode Observer Super-Twisting Algorithm," *2025 IEEE 12th International Symposium on Sensorless Control for Electrical Drives (SLED)*, pp. 1-6, 2025, https://doi.org/10.1109/SLED63792.2025.11154693.

[63] S. Liu, Q. Li, and Y. Zuo, "Research on SPMSM Vector Control Based on ADRC and SMC Under Multiple Operating Conditions," *Conference Proceedings of 2021 International Joint Conference on Energy, Electrical and Power Engineering*, pp. 305-315, 2022, https://doi.org/10.1007/978-981-19-3171-0_25.

[64] Q. Liu, M. Li, A. Wang, W. Ma, and S. Luo, "A Fast ADRC-SMC levitation control of EMS maglev train to suppress the vibration of electromagnet-track beam coupling system," *Measurement and Control*, 2025, https://doi.org/10.1177/00202940241312860.

[65] C. Liu, X. Xiang, Y. Duan, L. Yang, and S. Yang, "ADRC-SMC-based disturbance rejection depth-tracking control of underactuated AUV," *Journal of Field Robotics*, vol. 41, no. 4, pp. 1103-1115, 2024, https://doi.org/10.1002/rob.22312.

[66] Y. Choi, I. Joe, "Motor Fault Diagnosis and Detection with Convolutional Autoencoder (CAE) Based on Analysis of Electrical Energy Data," *Electronics*, vol. 13, no. 19, p. 3946, 2024, https://doi.org/10.3390/electronics13193946.

[67] K. Dawood and G. Komurgoz, "Investigating effect of Electromagnetic Force on Sandwich Winding Transformer using Finite Element Analysis," *2021 28th International Workshop on Electric Drives: Improving Reliability of Electric Drives (IWED)*, pp. 1-5, https://doi.org/10.1109/IWED52055.2021.9376371.

[68] H. Van Doan, "Adaptive Sliding Mode Control for Trajectory Tracking in Three-Wheeled Mobile Robots: Experimental Validation and Performance Analysis," *Journal of Robotics and Control (JRC)*, vol. 6, no. 4, pp. 1758-1767, 2025, https://doi.org/10.18196/jrc.v6i4.25570.

[69] D. Q. Du and T. D. Chuyen, "Design of a Novel Observer-Based SMC for WECS System Using PMSG to Obtain Maximum Energy," *Journal of Robotics and Control (JRC)*, vol. 6, no. 2, pp. 871-979, 2025, https://doi.org/10.18196/jrc.v6i2.25990.

[70] A. Al-Tamimi and T. MohammadRidha, “Adaptive Sliding Mode Control for Structural Vibration Using Magnetorheological Damper,” *Journal of Robotics and Control (JRC)*, vol. 6, no. 3, pp. 1308-1315, 2025, https://doi.org/10.18196/jrc.v6i3.26435.

[71] D. Acharya and D. K. Das, "Human Conception Optimizer-Based Optimal Type-2 Fuzzy PID Controller Design for Artificial Respiratory System," *IEEE Transactions on Systems, Man, and Cybernetics: Systems*, vol. 54, no. 9, pp. 5388-5399, 2024, https://doi.org/10.1109/TSMC.2024.3406594.

[72] J. Arcos-Legarda and A. Tovar, “Mechatronic Design and Active Disturbance Rejection Control of a Bag Valve-Based Mechanical Ventilator,” *Journal of Medical Devices*, vol. 15, no. 3, p. 031006, 2021, https://doi.org/10.1115/1.4051064.

[73] A. Tang, L. Yang, T. Zeng, Q. Yu, “Cascade Control Method of Sliding Mode and PID for PEMFC Air Supply System,” *Energies*, vol. 16, no. 1, p. 228, 2023, https://doi.org/10.3390/en16010228.

[74] M. Adwaith Narayan and R. K. Megalingam, "FPGA Based PWM Controlled Air Ventillation System Using PID, Fuzzy Control And Adaptive PID," *2025 8th International Conference on Circuit, Power & Computing Technologies (ICCPCT)*, pp. 375-381, 2025, https://doi.org/10.1109/ICCPCT65132.2025.11176746.